

Topological transverse transport in the presence and absence of long-range magnetic order in EuCd_2As_2

Y. Xu,^{1,*} L. Das,¹ J. Z. Ma,² C. J. Yi,^{3,4} Y. G. Shi,³ A. Tiwari,^{1,5} S. S. Tsirkin,¹ T. Neupert,¹ M. Medarde,⁶ M. Shi,² J. Chang,^{1,†} and T. Shang^{1,6,‡}

¹*Physik-Institut, Universität Zürich, Winterthurerstrasse 190, CH-8057 Zürich, Switzerland*

²*Swiss Light Source, Paul Scherrer Institut, Villigen CH-5232, Switzerland*

³*Beijing National Laboratory for Condensed Matter Physics,*

Institute of Physics, Chinese Academy of Sciences, Beijing 100190, China

⁴*University of Chinese Academy of Sciences, Beijing 100049, China*

⁵*Condensed Matter Theory Group, Paul Scherrer Institute, CH-5232 Villigen PSI, Switzerland*

⁶*Laboratory for Multiscale Materials Experiments,*

Paul Scherrer Institut, CH-5232 Villigen PSI, Switzerland

(Dated: August 13, 2020)

As exemplified by the growing interest in the quantum anomalous Hall effect, the research on topology as an organizing principle of quantum matter is greatly enriched from the interplay with magnetism. In this vein, we present a combined electrical and thermoelectrical transport study on the magnetic Weyl semimetal EuCd_2As_2 . Topological Hall and topological Nernst effects were observed in both the antiferromagnetic and the paramagnetic phase of EuCd_2As_2 , indicating the existence of significant Berry curvature. EuCd_2As_2 represents a rare case in which the topological transverse transport emerges both in the presence and absence of long-range magnetic order in the same material. The transport properties evolve with temperature and field in the antiferromagnetic phase in a different manner than in the paramagnetic phase, suggesting different mechanisms to their origin. Our results indicate EuCd_2As_2 is a fertile playground for investigating the interplay between magnetism and topology, and potentially a plethora of topologically nontrivial phases rooted in this interplay.

The last few decades have witnessed the effort of researchers seeking unique insights into the physics of materials from the view of topology. When magnetism, the most time-honored branch in condensed matter physics, is incorporated into this view, novel phenomena are to be expected. One notable manifestation is an additional contribution to transverse transport effects. For example, the topological Hall effect (THE) has been intensively studied in systems exhibiting non-coplanar spin textures with finite scalar spin chirality, such as skyrmions [1–11], hedgehogs [12, 13], hopfions [14], merons [15], and magnetic bubbles [16]. Alternative to this real-space scenario, THE has also been observed in systems with momentum-space anomalies such as Weyl points near the Fermi level, which carry significant Berry curvature that acts like an effective magnetic field in the momentum space [17–23].

It has been demonstrated recently that the antiferromagnet EuCd_2As_2 with $T_N \sim 9.5$ K would be an ideal candidate for the study of the interplay between magnetism and topology, as it exhibits various topological orders in both the antiferromagnetic (AFM) and paramagnetic (PM) phases [24–29]. In the AFM phase, depending on the direction of the Eu magnetic moments, various nontrivial topological ground states have been predicted, such as magnetic topological Dirac semimetal, or axion insulator, AFM topological crystalline insulator, and higher order topological insulator [28]. When the spins are aligned along the c axis by external magnetic field, a single pair of Weyl points appears near the Fermi level [26, 28]. In the PM phase, EuCd_2As_2 turns out to

be the first discovered centrosymmetric Weyl semimetal where ferromagnetic spin fluctuations, instead of long-range magnetic order, lift the Kramers degeneracy [25]. A rich H - T (magnetic field versus temperature) phase diagram is thus expected for EuCd_2As_2 [24, 26–28]. Profound insights into the interplay between magnetism and topology, from the exploration of this phase diagram in the context of topological transport, can be reasonably foreseen and, thus, such a transport study is highly desired.

Thermoelectrical transport can provide additional information than electrical transport, as it is usually more sensitive to the Berry curvature near the Fermi level [30]. As a thermoelectrical counterpart of the THE, the topological Nernst effect (TNE) has only been reported in few systems [21, 22, 31–33]. Linked to each other by the Mott relation [32], the observation of a large THE, however, does not guarantee a large TNE [31, 34]. Here, we present a systematic study of the electrical and thermoelectrical transport properties of EuCd_2As_2 . The observation of THE and TNE in the PM phase in EuCd_2As_2 represents a rare case of topological transverse transport beyond the ordinary and conventional anomalous contribution in the absence of long-range magnetic order. In the PM phase, both positive and negative THE and TNE were observed and attributed to the fluctuating Weyl points near the Fermi level. In the AFM phase, the THE and TNE evolve with field and temperature in a qualitatively different manner compared to that in the PM phase, and their origins may be attributed to a concerted effort from

the real-space and momentum-space scenarios contributing to the Berry curvature.

Single crystals of EuCd_2As_2 were grown by a Sn flux method [25]. The single crystals were cut and polished into a rectangular shape, with the largest natural plane being the ab plane. Magnetic fields $\mu_0 H$ (μ_0 being the vacuum permeability) up to 9 T were applied along the c axis, while electrical and thermal currents, and the measured voltage drops were all in the ab plane. Magnetization and electrical transport measurements were performed in a Quantum Design magnetic property measurement system (MPMS) and a physical property measurement system (PPMS), respectively, while thermoelectrical transport measurements were performed with a home-built probe integrated to the PPMS. The temperature gradient in the sample was held at $\sim 3\%$ of the sample temperature and was measured with Cernox thermometers, while the voltage was measured using nanovoltmeters.

The magnetic field dependence of the magnetization M , longitudinal resistivity ρ_{xx} , Hall resistivity ρ_{xy} , and Nernst signal S_{xy} of EuCd_2As_2 for different temperatures are shown in Fig 1. Anomalies in the low field region are already evident in these isotherms without further processing. For transverse transport ρ_{xy} and S_{xy} , the most prominent feature is the presence of low-field peaks superimposed on a (quasi-) linear background. Both the associated field scale and amplitude of the peaks exhibit a strong variation with temperature. For each isotherm, the empirical relation $\rho_{xy} = \rho_{xy}^O + \rho_{xy}^A + \rho_{xy}^T = R_0\mu_0 H + S_H\rho_{xx}^2 M + \rho_{xy}^T$ were applied to separate the different contributions to ρ_{xy} . The additivity of the above relation holds for $\rho_{xy} \ll \rho_{xx}$ [4], which is the case here in EuCd_2As_2 [Fig. 1(b) and (c)]. Here, R_0 and S_H are constants for a given isotherm, and the three terms in the relation are the ordinary, conventional anomalous, and topological Hall contribution, respectively. The form of ρ_{xy}^A used here assumes the domination of the intrinsic mechanism for the conventional anomalous Hall effect [35, 36]. Assuming instead a skew scattering dominated ρ_{xy}^A barely affects the results (see Sec. II in the Supplemental Material [37]). This decomposition procedure is shown in Fig. 2(a), and the derived THE term ρ_{xy}^T are shown in Fig. 2(b). The Nernst conductivity α_{xy} is obtained using $\alpha_{xy} = \sigma_{xx}S_{xy} + \sigma_{xy}S_{xx} + \sigma_{xx}\kappa_H/\kappa$ [33, 38], where S_{xx} is the Seebeck signal (see Fig. S1), κ_H is the thermal Hall, and κ is the thermal conductivity (see Sec. III in the Supplemental Material [37]). As shown in Fig. 2(c), we employ similar procedure as that for ρ_{xy} to α_{xy} [33]: $\alpha_{xy} = \alpha_{xy}^O + \alpha_{xy}^A + \alpha_{xy}^T = Q_0\mu_0 H + Q_s M + \alpha_{xy}^T$, with Q_0 and Q_s being constants for a specific isotherm. The resulting isotherms of the TNE term α_{xy}^T are shown in Fig. 2(d). The temperature dependence of the amplitude of the positive and negative peaks of ρ_{xy}^T and α_{xy}^T are summarized in Fig. 3(a). The peak posi-

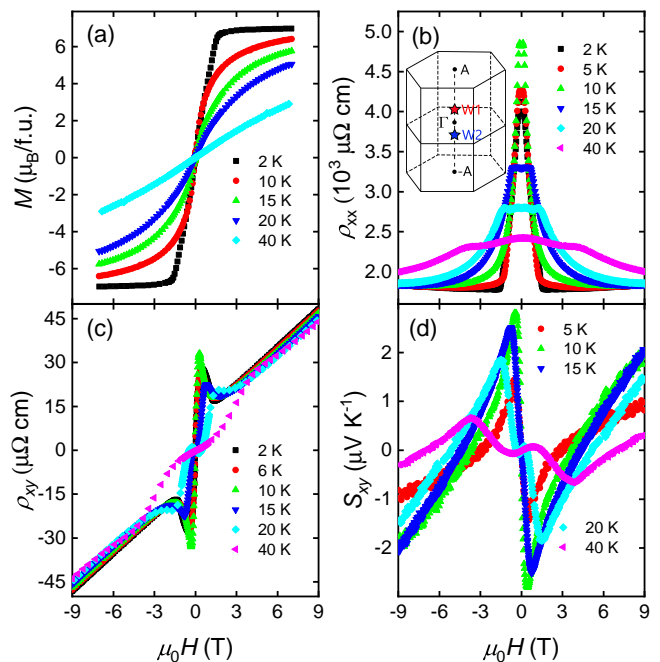


FIG. 1. The magnetic field dependence of the (a) magnetization M , (b) resistivity ρ_{xx} , (c) Hall resistivity ρ_{xy} , and (d) Nernst signal S_{xy} of EuCd_2As_2 for selected temperatures. The ρ_{xx} isotherms are symmetrized while the ρ_{xy} and S_{xy} isotherms antisymmetrized. The inset of (b) illustrates the locations of a single pair of Weyl points (W1 and W2) in the Brillouin zone.

tions at different temperatures are superimposed on the contour plot of ρ_{xy}^T in Fig. 3(b), forming a rich $H - T$ phase diagram of EuCd_2As_2 covering both the AFM and PM phase. Apart from a bifurcation of peak positions at low temperatures [Fig. 3(b)], the electrical and thermoelectrical transport properties are consistent and, thus, corroborate each other.

Considering the observations in Figs. 2(b) and 2(d), and in Figs. 3(a) and 3(b), it is clear that both ρ_{xy}^T and α_{xy}^T exhibit a two-stage evolution, *i.e.*, they evolve in a qualitatively different manner in the AFM phase compared to in the PM phase: (i) The field scale associated with the positive peak decreases with increasing temperature in the AFM phase while it increases in the PM phase. As a result, the field scale of the 10 K (slightly above T_N) isotherm is the smallest among all the isotherms (ii) The width of the positive peak decreases with increasing temperature in the AFM phase while it increases in the PM phase (iii) The amplitude of the positive peak decreases with increasing temperature both in the AFM and PM phase, but there is a sudden increase around T_N , such that the 10 K isotherm exhibits a peak amplitude larger than any of the isotherms in the AFM phase (iv) The negative peak is only observed in the PM phase. As temperature increases in the PM phase, the positive peak

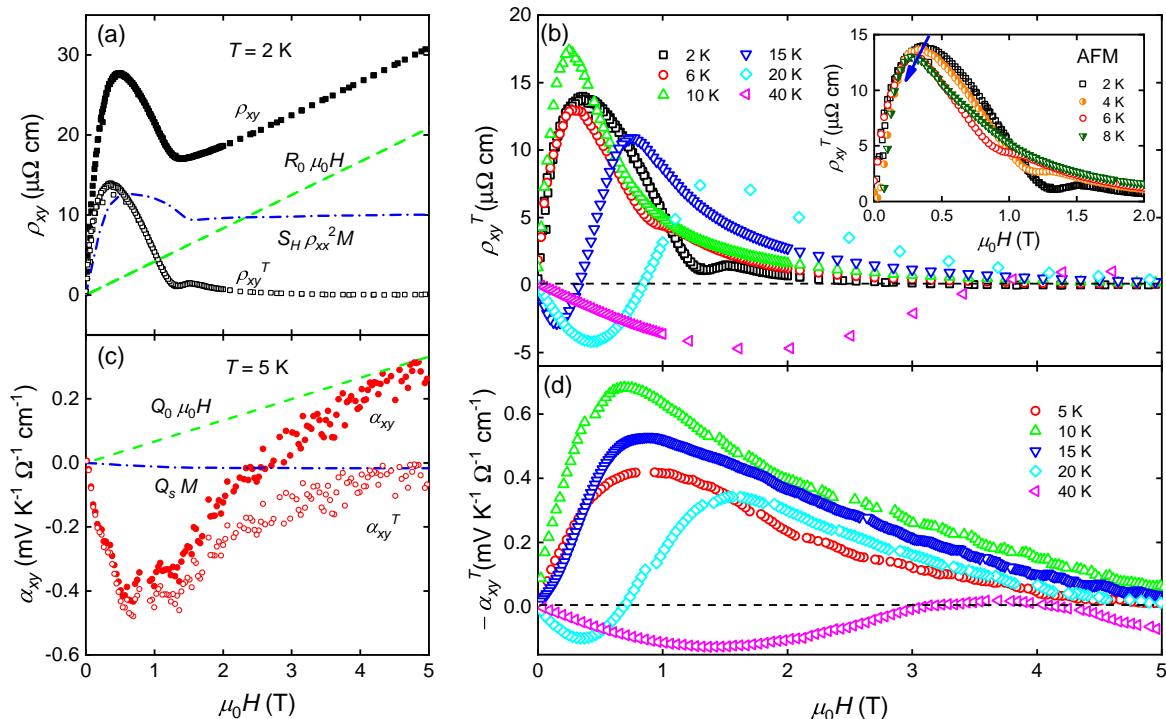


FIG. 2. (a,c) The decomposition procedure of the Hall resistivity ρ_{xy} and Nernst conductivity α_{xy} into different components, exemplified by the lowest temperature isotherm. (b,d) The magnetic field dependence of the topological Hall resistivity ρ_{xy}^T and the topological Nernst conductivity $-\alpha_{xy}^T$ for selected temperatures. The isotherms are shown for $\mu_0 H \leq 5$ T, since they are basically featureless at higher fields. The inset of (b) shows an enlarged view of the positive peak on the ρ_{xy}^T isotherms in the antiferromagnetic phase. The blue arrow tracks the evolution of the peak with increasing temperature.

gradually gives way to a negative peak. All these observations indicate different origins of the THE and TNE in the AFM and PM phase.

We first discuss the THE and TNE in the PM phase. A combined study of angle-resolved photoemission spectroscopy and first-principles calculation identified a pair of Weyl points near the Fermi level along the $\Gamma - A$ high symmetry line in EuCd_2As_2 [see the inset of Fig. 1(b)], whose origin was attributed to the effective time-reversal-symmetry breaking by quasi-static and quasi-long-range ferromagnetic fluctuations [25]. Since Weyl points are sources of Berry curvature in the momentum space, they are expected to give rise to THE and TNE, as in the case of both the THE and TNE in Mn_3Sn [19, 31] (for $T \geq 20$ K, at lower temperatures a real-space mechanism sets in [39]), Cd_3As_2 [20, 21], and ZrTe_5 [22], the THE in GdPtBi [23], YbPtBi [40], and Mn_3Ge [41], and the TNE in TaAs [42], TaP [42], and NbP [43]. The THE and TNE reported up to date are mostly observed in the presence of long-range magnetic order or applied magnetic field. In GdPtBi , although a finite THE above T_N was observed, it necessitates the application of a finite magnetic field to break the combined time-reversal and lattice symmetries [23]. In nonmagnetic topological semimetals Cd_3As_2 , ZrTe_5 , TaAs , TaP , and NbP , a finite

magnetic field is also required to split the Dirac point into Weyl points, or to tune the Weyl points close to the Fermi level [20–22, 42, 43]. In contrast, in the PM phase of EuCd_2As_2 , as the time-reversal symmetry is broken by spin fluctuations, the Weyl points are already lying in the vicinity of the Fermi level even at zero field [25]. In principle, the PM phase of EuCd_2As_2 represents an uncommon case where neither long-range magnetic order nor applied magnetic field is needed to promote the topological transverse transport, although experimentally no spontaneous transverse signal was observed at zero field, probably due to its small value (see Sec. V in the Supplemental Material [37]). In the chiral spin liquid $\text{Pr}_2\text{Ir}_2\text{O}_7$, THE was observed without magnetic order or external field [44], but only for $T \leq 1.5$ K. By contrast, we could identify the THE and TNE up to at least 40 K in the PM phase of EuCd_2As_2 . Furthermore, EuCd_2As_2 is a rare case in which the THE and TNE can be observed both in the presence and absence of long-range magnetic order in the same material. THE across T_N was also observed in GdPtBi and YbPtBi [23, 40]. However, there the THE gets diminished monotonically with increasing temperature, with no anomaly around T_N , pointing to a single underlying mechanism at all temperatures [23, 40], as opposed to the two-stage behavior in EuCd_2As_2 .

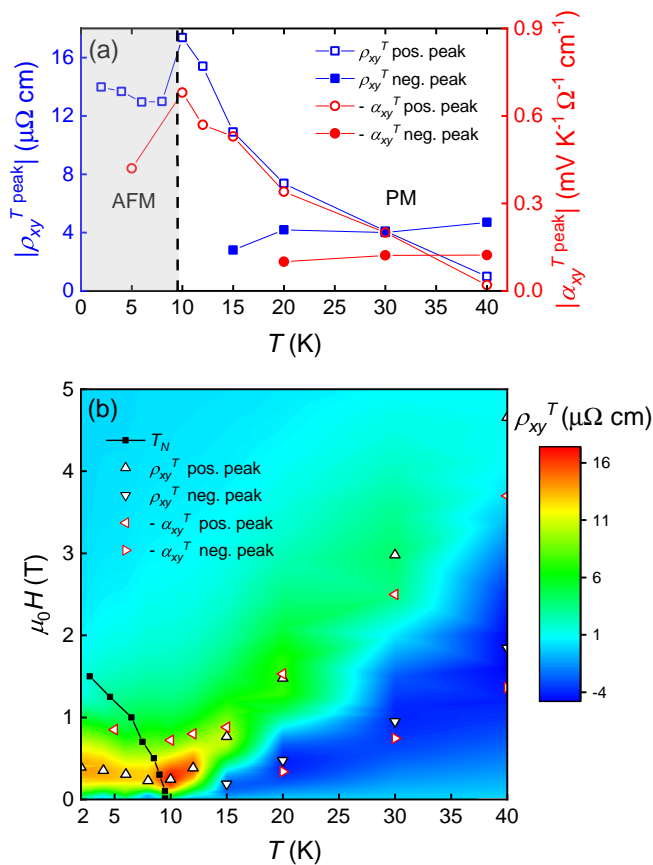


FIG. 3. (a) Temperature dependence of the absolute values of ρ_{xy}^T (blue squares, left axis) and α_{xy}^T (red circles, right axis) at the positive peak (open symbols) and negative peak (filled symbols). The vertical dashed line separates the antiferromagnetic and the paramagnetic phase. (b) The H - T (magnetic field versus temperature) phase diagram of EuCd_2As_2 . The colors represent the magnitude of the topological Hall resistivity ρ_{xy}^T . The Néel temperatures T_N are extracted from susceptibility measurements (see Fig. S1). The positions of the positive and negative peaks of ρ_{xy}^T (upper and lower triangles) and $-\alpha_{xy}^T$ (left and right triangles) are also superimposed.

Another notable feature of the THE and TNE in the PM phase of EuCd_2As_2 is the coexistence of positive and negative values. The possible mechanism of this is discussed in Sec. VI in the Supplemental Material [37]. The fact that the THE and TNE of both signs were observed in the PM phase, and that they originate from Weyl points induced by spin fluctuations present already at zero field, give EuCd_2As_2 in its PM phase a unique place among magnetic topological materials.

We now turn to the THE and TNE in the AFM phase. It was proposed that EuCd_2As_2 exhibits an A-type AFM structure, in which the spins form ferromagnetic layers which stack antiferromagnetically along the c axis [45–47]. At zero field, the moments lie in the ab plane. When

a finite external magnetic field aligns the moments along the c axis, a pair of Weyl points along the $\Gamma - A$ line emerge associated with the restoration of the C_3 symmetry [24, 26–28], giving rise to the THE and TNE. Although this mechanism of Weyl points giving rise to THE and TNE appears similar to the case of the PM phase, the two-stage evolution calls for a more complex picture: a) If there is only the momentum-space scenario of Weyl points at play in the AFM phase, the resultant Berry curvature must be different than that in the PM phase, due to the interplay with the long-range AFM order. This interplay gradually fades away accompanied by the disappearance of the folded bands in the AFM phase with increasing temperature [28] in the AFM phase. Around T_N , the mechanism of spin fluctuation induced Weyl points sets in, leading to a discontinuity in the peak amplitude of the THE and TNE across T_N [Fig. 3(a)]. b) There are features that cannot be explained solely by the Weyl points mechanism, hinting at other mechanisms at play. For example, at 2 K, the magnetic field needed to align the spins along the c axis as seen in the magnetization is ~ 2 T, while the THE peaks around 0.4 T. In fact, the AFM portion of the phase diagram shown in Fig. 3(b) strongly resembles that of systems with a real-space scenario induced THE. For instance, in Gd_2PdSi_3 , a skyrmion lattice phase is sandwiched by two incommensurate spin-state phases, and a finite ρ_{xy}^T can only be observed in the skyrmion lattice phase [11]. The ρ_{xy}^T peak also exhibits an amplitude, field scale, and width that decrease with increasing temperature [11], as is the case in the AFM phase of EuCd_2As_2 . Based on our results alone, a contribution from a real-space scenario can neither be pinned down nor excluded in the AFM phase of EuCd_2As_2 [48]. The genuine magnetic structure of EuCd_2As_2 under magnetic field could be complex, considering the sizable frustration in this material [25]. In view of the technical difficulty in performing neutron diffraction measurement on EuCd_2As_2 [45], real-space probes such as Lorentz transmission electron microscopy are required to search for potential spin textures with finite chirality. We note that the AFM topological insulator MnBi_2Te_4 , which also exhibits frustration and an A-type AFM order with triangular layers of magnetic atoms, has been recently predicted to realize a skyrmion phase under magnetic field [49].

Finally we compare the magnitude of the THE and TNE in EuCd_2As_2 with other systems. In a real-space scenario, the $|\rho_{xy}^T|^{\text{max}} \sim 20 \mu\Omega \text{ cm}$ reported here in EuCd_2As_2 is significant, as compared to, *e.g.*, the so-called giant THE in Gd_2PdSi_3 with $|\rho_{xy}^T|^{\text{max}} \sim 3 \mu\Omega \text{ cm}$ [11]. In a momentum-space scenario, it is more appropriate to compare the magnitude of σ_{xy}^T and the topological Hall angle $\Theta_H^T = \sigma_{xy}^T / \sigma_{xx}^T$ [18]. The $|\sigma_{xy}^T|^{\text{max}} \sim 1 \Omega^{-1} \text{ cm}^{-1}$ and $|\Theta_H^T|^{\text{max}} \sim 0.01$ (see Sec. IV in the Supplemental Material [37]) reported here in EuCd_2As_2

Compound	$ \alpha_{xy}^T/T ^{\max}$ (10^{-2} A K $^{-2}$ m $^{-1}$)	Origin
EuCd ₂ As ₂ (AFM)	0.8 [This work]	k -space (+ r -space?)
EuCd ₂ As ₂ (PM)	0.7 [This work]	k -space
Mn ₃ Sn	0.2 [31]	k -space
Gd ₂ PdSi ₃	3.5 [32]	r -space
MnGe	2.3 [33]	r -space
MnSi	0.3 [32]	r -space

TABLE I. **Comparison of the magnitude of the topological Nernst effect in various materials.** k -space stands for a momentum-space scenario, while r -space stands for a real-space scenario. In Mn₃Sn, the topological Nernst effect mentioned here is referred to as anomalous Nernst effect in the literature, see Footnote [17].

are comparable to the values estimated from a previous study [26], and are one order of magnitude smaller than that in GdPtBi [23]. In Table 1, we compare the TNE $|\alpha_{xy}^T/T|^{\max}$ in several systems and their origins. It is worth noting that the TNE in EuCd₂As₂ is larger than the Weyl-point-induced TNE in Mn₃Sn [31].

The ample features in the transport and the consequent rich phase diagram put strong constraints on the theoretical description of EuCd₂As₂. For example, in certain cases the contribution to the transverse transport generated by a pair of Weyl points is proportional to the distance between them [50]. The applicability of this relation in EuCd₂As₂ was briefly discussed in Ref. [26]. Theory should capture how the distance is varied with temperature and field to reproduce the phase diagram as observed here [51]. Such studies are expected to provide exciting insights, considering how a variety of topologically nontrivial phases have been predicted already at zero field [28]. The traversal among these, and conceivably more, topologically nontrivial phases, may also be achieved by symmetry-breaking perturbations other than applied magnetic fields, leaving room for the exploitation of more diverse means of tuning [43, 52, 53]. As an intriguing example, a gate-controllable topological phase transition between quantum anomalous Hall and time-reversal symmetry broken quantum spin Hall states has been recently predicted in quintuple-layer EuCd₂As₂ [52].

In summary, our electrical and thermoelectrical transport measurements on EuCd₂As₂ produce highly consistent results: topological Hall effect and topological Nernst effect are revealed both below and above the antiferromagnetic ordering temperature T_N . The topological terms are most likely associated with the Weyl points near the Fermi level, both below and above T_N , although in the former case a contribution from topological real-space spin textures may also need to be invoked. The

existence of a topological term above T_N is in itself uncommon. Moreover, the two-stage evolution of the topological term in the antiferromagnetic and in the paramagnetic phase hints at their different mechanism originating from the interplay of magnetism and topology.

Y. X., J. C., and T. Shang were financially supported by the Swiss National Science Foundation (SNSF) (Grant No. PP00P2_179097 and 206021_139082). L. D. was partially funded through Excellence Scholarship by the Swiss Government. C. J. Yi and Y. G. Shi acknowledged the support from the National Key Research and Development Program of China (No. 2017YFA0302901), and the K. C. Wong Education Foundation (GJTD-2018-01). A. Tiwari received funding from the European Research Council (ERC) under the Marie Skłodowska-Curie grant agreement No. 701647. S. S. T. and T. N. acknowledge support from NCCR Marvel and from the European Unions Horizon 2020 research and innovation program (ERC-StG-Neupert-757867-PARATOP). S. S. T. also acknowledges support from the Swiss National Science Foundation (Grant No. PP00P2_176877).

* yangxu@physik.uzh.ch

† johan.chang@physik.uzh.ch

‡ tian.shang@psi.ch

- [1] A. Neubauer, C. Pfleiderer, B. Binz, A. Rosch, R. Ritz, P. G. Niklowitz, and P. Böni, *Phys. Rev. Lett.* **102**, 186602 (2009).
- [2] J. Gayles, F. Freimuth, T. Schena, G. Lani, P. Mavropoulos, R. A. Duine, S. Blügel, J. Sinova, and Y. Mokrousov, *Phys. Rev. Lett.* **115**, 036602 (2015).
- [3] M. Lee, W. Kang, Y. Onose, Y. Tokura, and N. P. Ong, *Phys. Rev. Lett.* **102**, 186601 (2009).
- [4] N. Kanazawa, Y. Onose, T. Arima, D. Okuyama, K. Ohoyama, S. Wakimoto, K. Kakurai, S. Ishiwata, and Y. Tokura, *Phys. Rev. Lett.* **106**, 156603 (2011).
- [5] Y. Li, N. Kanazawa, X. Z. Yu, A. Tsukazaki, M. Kawasaki, M. Ichikawa, X. F. Jin, F. Kagawa, and Y. Tokura, *Phys. Rev. Lett.* **110**, 117202 (2013).
- [6] C. Franz, F. Freimuth, A. Bauer, R. Ritz, C. Schnarr, C. Duvinage, T. Adams, S. Blügel, A. Rosch, Y. Mokrousov, and C. Pfleiderer, *Phys. Rev. Lett.* **112**, 186601 (2014).
- [7] S. X. Huang and C. L. Chien, *Phys. Rev. Lett.* **108**, 267201 (2012).
- [8] T. Schulz, R. Ritz, A. Bauer, M. Halder, M. Wagner, C. Franz, C. Pfleiderer, K. Everschor, M. Garst, and A. Rosch, *Nat. Phys.* **8**, 301 (2012).
- [9] Q. Qin, L. Liu, W. Lin, X. Shu, Q. Xie, Z. Lim, C. Li, S. He, G. M. Chow, and J. Chen, *Adv. Mater.* **31**, 1807008 (2019).
- [10] J. Matsuno, N. Ogawa, K. Yasuda, F. Kagawa, W. Koshibae, N. Nagaosa, Y. Tokura, and M. Kawasaki, *Sci. Adv.* **2**, e1600304 (2016).
- [11] T. Kurumaji, T. Nakajima, M. Hirschberger, A. Kikkawa, Y. Yamasaki, H. Sagayama, H. Nakao, Y. Taguchi, T.-h. Arima, and Y. Tokura, *Science* **365**,

- 914 (2019).
- [12] N. Kanazawa, Y. Nii, X.-X. Zhang, A. S. Mishchenko, G. De Filippis, F. Kagawa, Y. Iwasa, N. Nagaosa, and Y. Tokura, *Nat. Commun.* **7**, 1 (2016).
- [13] Y. Fujishiro, N. Kanazawa, T. Nakajima, X. Z. Yu, K. Ohishi, Y. Kawamura, K. Kakurai, T. Arima, H. Mitamura, A. Miyake, K. Akiba, M. Tokunaga, A. Matsuo, K. Kindo, T. Koretsune, R. Arita, and Y. Tokura, *Nat. Commun.* **10**, 1 (2019).
- [14] B. Göbel, C. A. Akosa, G. Tatara, and I. Mertig, *Phys. Rev. Research* **2**, 013315 (2020).
- [15] P. Puphal, V. Pomjakushin, N. Kanazawa, V. Ukleev, D. J. Gawryluk, J. Ma, M. Naamneh, N. C. Plumb, L. Keller, R. Cubitt, E. Pomjakushina, and J. S. White, *Phys. Rev. Lett.* **124**, 017202 (2020).
- [16] L. Vistoli, W. Wang, A. Sander, Q. Zhu, B. Casals, R. Cichelero, A. Barthélémy, S. Fusil, G. Herranz, S. Valencia, R. Abrudan, E. Weschke, K. Nakazawa, H. Kohno, J. Santamaria, W. Wu, V. Garcia, and M. Bibes, *Nat. Phys.* **15**, 67 (2019).
- [17] In the momentum-space scenario, the term ‘anomalous Hall (Nernst) effect’ is more often used in the literature to denote any contribution other than the ordinary Hall (Nernst). To avoid confusion, here we use ‘topological Hall (Nernst) effect’ to denote the contribution in addition to the ordinary Hall (Nernst) and the *conventional* anomalous Hall (Nernst) that is proportional to magnetization, regardless of whether it originates from a real-space or momentum-space scenario. In other words, the topological Hall (Nernst) effect as we defined here is the topologically nontrivial part of the anomalous Hall (Nernst).
- [18] M. Onoda, G. Tatara, and N. Nagaosa, *J. Phys. Soc. Jpn.* **73**, 2624 (2004).
- [19] S. Nakatsuji, N. Kiyohara, and T. Higo, *Nature* **527**, 212 (2015).
- [20] T. Liang, Q. Gibson, M. N. Ali, M. Liu, R. J. Cava, and N. P. Ong, *Nat. Mater.* **14**, 280 (2015).
- [21] T. Liang, J. Lin, Q. Gibson, T. Gao, M. Hirschberger, M. Liu, R. J. Cava, and N. P. Ong, *Phys. Rev. Lett.* **118**, 136601 (2017).
- [22] T. Liang, J. Lin, Q. Gibson, S. Kushwaha, M. Liu, W. Wang, H. Xiong, J. A. Sobota, M. Hashimoto, P. S. Kirchmann, Z.-X. Shen, R. J. Cava, and N. P. Ong, *Nat. Phys.* **14**, 451 (2018).
- [23] T. Suzuki, R. Chisnell, A. Devarakonda, Y.-T. Liu, W. Feng, D. Xiao, J. W. Lynn, and J. G. Checkelsky, *Nat. Phys.* **12**, 1119 (2016).
- [24] G. Hua, S. Nie, Z. Song, R. Yu, G. Xu, and K. Yao, *Phys. Rev. B* **98**, 201116(R) (2018).
- [25] J.-Z. Ma, S. M. Nie, C. J. Yi, J. Jandke, T. Shang, M. Y. Yao, M. Naamneh, L. Q. Yan, Y. Sun, A. Chikina, V. N. Strocov, M. Medarde, M. Song, Y.-M. Xiong, G. Xu, W. Wulfschel, J. Mesot, M. Reticcioli, C. Franchini, C. Mudry, M. Müller, Y. G. Shi, T. Qian, H. Ding, and M. Shi, *Sci. Adv.* **5**, eaaw4718 (2019).
- [26] J.-R. Soh, F. de Juan, M. G. Vergniory, N. B. M. Schröter, M. C. Rahn, D. Y. Yan, J. Jiang, M. Bristow, P. Reiss, J. N. Blandy, Y. F. Guo, Y. G. Shi, T. K. Kim, A. McCollam, S. H. Simon, Y. Chen, A. I. Coldea, and A. T. Boothroyd, *Phys. Rev. B* **100**, 201102(R) (2019).
- [27] L.-L. Wang, N. H. Jo, B. Kuthanazhi, Y. Wu, R. J. McQueeney, A. Kaminski, and P. C. Canfield, *Phys. Rev. B* **99**, 245147 (2019).
- [28] J. Ma, H. Wang, S. Nie, C. Yi, Y. Xu, H. Li, J. Jandke, W. Wulfschel, Y. Huang, D. West, P. Richard, A. Chikina, V. N. Strocov, J. Mesot, H. Weng, S. Zhang, Y. Shi, T. Qian, M. Shi, and H. Ding, *Adv. Mater.* **32**, 1907565 (2020).
- [29] N. H. Jo, B. Kuthanazhi, Y. Wu, E. Timmons, T.-H. Kim, L. Zhou, L.-L. Wang, B. G. Ueland, A. Palasyuk, D. H. Ryan, R. J. McQueeney, K. Lee, B. Schrunck, A. A. Burkov, R. Prozorov, S. L. Bud’ko, A. Kaminski, and P. C. Canfield, *Phys. Rev. B* **101**, 140402(R) (2020).
- [30] K. Behnia and H. Aubin, *Rep. Prog. Phys.* **79**, 046502 (2016).
- [31] M. Ikhlas, T. Tomita, T. Koretsune, M.-T. Suzuki, D. Nishio-Hamane, R. Arita, Y. Otani, and S. Nakatsuji, *Nat. Phys.* **13**, 1085 (2017).
- [32] M. Hirschberger, L. Spitz, T. Nakajima, T. Kurumaji, A. Kikkawa, Y. Taguchi, and Y. Tokura, [arXiv:1910.06027](https://arxiv.org/abs/1910.06027).
- [33] Y. Shiomi, N. Kanazawa, K. Shibata, Y. Onose, and Y. Tokura, *Phys. Rev. B* **88**, 064409 (2013).
- [34] D. Xiao, M.-C. Chang, and Q. Niu, *Rev. Mod. Phys.* **82**, 1959 (2010).
- [35] M. Lee, Y. Onose, Y. Tokura, and N. P. Ong, *Phys. Rev. B* **75**, 172403 (2007).
- [36] N. Nagaosa, J. Sinova, S. Onoda, A. H. MacDonald, and N. P. Ong, *Rev. Mod. Phys.* **82**, 1539 (2010).
- [37] See Supplemental Material for more characterizations of the sample, discussions on the decomposition procedure of the topological Hall resistivity and conductivity, discussions about obtaining the Nernst conductivity, a possible explanation for the absence of a zero-field topological term in transport, and discussions about the topological transport of both positive and negative values, which includes Refs. [4, 12, 13, 25, 26, 28, 33, 35, 36, 38, 43, 45, 50, 54, 55].
- [38] Y. Onose, L. Li, C. Petrovic, and N. P. Ong, *EPL* **79**, 17006 (2007).
- [39] P. K. Rout, P. V. P. Madduri, S. K. Manna, and A. K. Nayak, *Phys. Rev. B* **99**, 094430 (2019).
- [40] C. Y. Guo, F. Wu, Z. Z. Wu, M. Smidman, C. Cao, A. Bostwick, C. Jozwiak, E. Rotenberg, Y. Liu, F. Steglich, and H. Q. Yuan, *Nat. Commun.* **9**, 4622 (2018).
- [41] A. K. Nayak, J. E. Fischer, Y. Sun, B. Yan, J. Karel, A. C. Komarek, C. Shekhar, N. Kumar, W. Schnelle, J. Kübler, C. Felser, and S. S. P. Parkin, *Sci. Adv.* **2**, e1501870 (2016).
- [42] F. Caglieris, C. Wuttke, S. Sykora, V. Süß, C. Shekhar, C. Felser, B. Büchner, and C. Hess, *Phys. Rev. B* **98**, 201107(R) (2018).
- [43] S. J. Watzman, T. M. McCormick, C. Shekhar, S.-C. Wu, Y. Sun, A. Prakash, C. Felser, N. Trivedi, and J. P. Heremans, *Phys. Rev. B* **97**, 161404(R) (2018).
- [44] Y. Machida, S. Nakatsuji, S. Onoda, T. Tayama, and T. Sakakibara, *Nature* **463**, 210 (2010).
- [45] M. C. Rahn, J.-R. Soh, S. Francoual, L. S. I. Veiga, J. Stremper, J. Mardegan, D. Y. Yan, Y. F. Guo, Y. G. Shi, and A. T. Boothroyd, *Phys. Rev. B* **97**, 214422 (2018).
- [46] H. P. Wang, D. S. Wu, Y. G. Shi, and N. L. Wang, *Phys. Rev. B* **94**, 045112 (2016).
- [47] I. Schellenberg, U. Pfannenschmidt, M. Eul, C. Schwickert, and R. Pöttgen, *Z. Anorg. Allg. Chem.* **637**, 1863 (2011).

- [48] One aspect in which a real-space scenario seems to be inconsistent with our results is, there should be kinks in the magnetization and peaks in the susceptibility isotherms corresponding to the border of, *e.g.*, a skyrmion lattice phase, in the $H - T$ phase diagram, since these borders represent metamagnetic transitions. Such kinks and peaks are not observed in our work, but it cannot be ruled out that the existence of them might be revealed by more detailed studies utilizing more sensitive probes of the magnetization and susceptibility.
- [49] B. Li, J.-Q. Yan, D. M. Pajerowski, E. Gordon, A.-M. Nedić, Y. Sizyuk, L. Ke, P. P. Orth, D. Vaknin, and R. J. McQueeney, [Phys. Rev. Lett. **124**, 167204 \(2020\)](#).
- [50] A. A. Burkov, [Phys. Rev. Lett. **113**, 187202 \(2014\)](#).
- [51] In this case, it is more appropriate to consider the values of the anomalous component, *i.e.*, the sum of the conventional anomalous and topological component in our notation. Such an $H - T$ phase diagram is shown in Fig. S2(b) [37].
- [52] C. Niu, N. Mao, X. Hu, B. Huang, and Y. Dai, [Phys. Rev. B **99**, 235119 \(2019\)](#).
- [53] L. D. Sanjeeva, J. Xing, K. M. Taddei, D. Parker, R. Custelcean, D. d. Cruz, and A. S. Sefat, [arXiv:2005.05217](#).
- [54] J.-R. Soh, E. Schierle, D.-Y. Yan, H. Su, D. Prabhakaran, E. Weschke, Y.-F. Guo, Y.-G. Shi, and A. Boothroyd, [arXiv:2005.04952](#).
- [55] H. Ishizuka and N. Nagaosa, [Sci. Adv. **4**, eaap9962 \(2018\)](#).